

Article

Apron and Cutoff Wall Scour Protection for Piano Key Weirs

Wyatt Lantz¹, Brian Mark Crookston^{1,*}  and Michele Palermo² 

¹ Utah Water Research Laboratory, Department Civil and Environmental Engineering, Utah State University, Logan, UT 84321, USA; wyatt.lantz@usu.edu

² DESTEC-Department of Energy, Systems, Territory and Construction Engineering, University of Pisa, 56122 Pisa, Italy; michele.palermo@ing.unipi.it

* Correspondence: brian.crookston@usu.edu; Tel.: +1-(435)-797-0247

Abstract: Piano key (PK) weirs are used in a variety of flow control structure applications, including spillway crests and open channel diversion structures. However, to the best of authors' knowledge, structure-specific design guidance for scour mitigation is still needed. To fill this gap of knowledge, a systematic experimental campaign was conducted by testing different configurations of horizontal aprons with a cutoff wall. Protection structures were located at the toe of the PK weir. Namely, experiments were performed at large-scale to assess the effect of three apron lengths on downstream scour hole geometry under different hydraulic conditions. It was observed that a horizontal apron deflects the plunging jets originating from the PK weir, thus significantly reducing scour. Experimental evidence allowed corroboration that significant scour depth reduction occurs for an apron length 1.5 times the weir height, with longer aprons found to provide marginal benefits. Finally, also provided herein are tools to estimate the main scour characteristics and help practitioners in optimizing apron design.

Keywords: horizontal apron; local scour; PK weir; scour countermeasure; vertical cutoff wall



Citation: Lantz, W.; Crookston, B.M.; Palermo, M. Apron and Cutoff Wall Scour Protection for Piano Key Weirs. *Water* **2021**, *13*, 2332. <https://doi.org/10.3390/w13172332>

Academic Editors: Jorge Matos, Sebastien Erpicum and Anton J. Schleiss

Received: 16 June 2021

Accepted: 20 August 2021

Published: 26 August 2021

Publisher's Note: MDPI stays neutral with regard to jurisdictional claims in published maps and institutional affiliations.



Copyright: © 2021 by the authors. Licensee MDPI, Basel, Switzerland. This article is an open access article distributed under the terms and conditions of the Creative Commons Attribution (CC BY) license (<https://creativecommons.org/licenses/by/4.0/>).

1. Introduction

When considering current design standards, sustainability principles, and observed trends in flooding, the control of local scour represents a challenging task. Therefore, the analysis of the interaction between catchment-based processes (e.g., runoff hydrographs, river morphology, and transport of sediments, and debris) and hydraulic structure functioning is of fundamental importance to minimize the risk of failure [1–5]. Weirs are a common hydraulic structure found in rivers and incorporated in dams and levees. Often, localized scour phenomena are caused by falling nappe or oblique plunging jets originating from weirs. Depending on jet characteristics (e.g., submergence, geometry, and inclination), scour morphology at equilibrium could be either two- or three-dimensional (considering the vertical and streamwise directions with the third dimension being transverse) [4–10].

Despite the numerous studies dealing with drop structures, including linear weirs, the scour process downstream of piano key (PK) weirs has been only recently analyzed and results are still insufficient to correctly assess such a complex phenomenon. Although design manuals, e.g., [11–17] can represent a valid help for practitioners with upstream and downstream erosion at PK weirs discussed in [18], none of them provide guidance for PK weirs' scour-induced processes and selection of a horizontal apron and cutoff wall for scour protection.

Nevertheless, PK weirs have become quite popular. They have been recently employed in a number of dam rehabilitation projects in Asia, Australia, Europe, and North America, as well as in some river restoration projects [19–21] (e.g., the run-of-river Van Phong PK weir in Vietnam). It was found that PK weirs perform well as in-channel flow control structures due to their hydraulic efficiency, do not require operation (passive flow control), possess construction economy, and have the ability to pass floating debris [22–25]. Following their

recent success in practical applications, there has been increased interest regarding scour morphology at PK weirs [6–31].

However, to date there are very few studies providing specific tools to estimate scour characteristics and, apparently, only one dealing with scour mitigation. More specifically, from scaled hydraulic models of structures in Vietnam, [19] suggested that PK and labyrinth weirs in rivers with high submergence only need a short stilling basin and end sill to dissipate energy. The authors of [27] investigated the scour formation downstream of PK weirs in a 0.67 m-wide channel (i.e., relatively narrow channel), providing some interesting insights on the erosion mechanism and useful empirical equations to predict the main geometric characteristics of the equilibrium morphology. Following this study, [28] focused on the design of a pre-excavated rip-rap apron. However, they did not provide comprehensive guidelines to design effective countermeasures to stabilize the stilling basin downstream of PK weir.

To fill this gap of knowledge, this study analyzed the scour process occurring downstream of a PK weir in the presence of downstream apron. This protection structure was selected because it is a simple and cost-effective alternative for scour mitigation. In addition, cutoff walls are commonly included with concrete aprons to prevent a failure mode via undermining of the slabs [32–35]. To this end, tests were conducted varying both the length of the apron and the height of the cutoff wall under different hydraulic conditions and with two bed materials. A dedicated, large-scale model was built at Utah State University. Experimental evidence allowed the assessment of the effect of protection structure geometry on the induced scour mechanism. Furthermore, this study provides unprecedented design guidelines that can represent a valid tool for practitioners.

2. Materials and Methods

A rectangular flume (16-m long, 2-m wide, and 1.8-m deep) was constructed at the Utah Water Research Laboratory. A transparent acrylic wall section allowed monitoring of the scour evolution. The flume provided uniform flows in the headbox to a Type A [36] PK weir via a diffuser pipe and rock baffling. A four-key acrylic PK weir was located in the flume whose dimensions are summarized in Table 1. The movable bed section downstream of the PK weir was 5 m long, 2 m wide, and 1.09 m deep. Tailwater was controlled with a stop log structure located 9.68 m downstream of the PK weir. Figure 1 shows diagram sketches of the experimental apparatus along with the main geometric parameters, where W = total PK weir width, B = depth of the PK weir, B_b = streamwise length of the base of the PK weir, B_i = the length of the inlet key, B_o = the length of the outlet key, S_o = slope of the outlet key, S_i = slope of the inlet key, W_u = cycle width, N = number of keys or cycles, P = weir height, T_s = sidewall thickness, W_i = width of the inlet key, W_o = width of the outlet key, P_d = height of the PK weir base relative to the invert of the channel, x_{M1} , x_{M2} , and x_{M3} are streamwise lengths from the apron to sphere measurement locations, L_a is the length of the apron, and L_c is the length or depth of the cutoff wall. Note that a false floor was not included upstream of the PK weir, as its presence would be negligible on the results of this study. We also note that the dimensions of the apron and cutoff wall are not indicative of actual thicknesses as may be structurally designed for specific applications.

Prior to each test, the movable bed was prepared to be level (zero bed slope) and at the elevation of the base of the PK weir. The various apron lengths and cutoff walls placed in the moveable bed were fabricated using dimensional lumber and coated for waterproofing. When the aprons were installed, they were also leveled at the elevation of the base of the PK weir, matching the bed surface.

Experimental tests involved two non-cohesive gravel substrates, i.e., Substrate 1 and 2. Substrate 1 was a coarse gravel with $d_{90} = 20.00$ mm, $d_{50} = 13.00$ mm, uniformity coefficient $\sigma = 1.54$, density $\rho_s = 2604$ kg/m³, and relative density $G = \rho_s / \rho = 2.61$, where d_{xx} is the diameter for which $xx\%$ is finer and ρ is the water density. Substrate 2 was a fine gravel with $d_{90} = 9.10$ mm, $d_{50} = 6.50$ mm, $\sigma = 1.30$, $\rho_s = 2604$ kg/m³, and $G = 2.61$. A diagram sketch illustrating the main hydraulic and scour parameters is shown in Figure 2, with

H indicating total hydraulic head ($H = h_u + V^2/2g$) where h_u is the depth of flow relative to the weir crest (with total weir crest length = L), g is the standard acceleration due to gravity, and V is an average upstream flow velocity. Figure 2 also shows the PK weir foundation height P_d , the change in energy head, ΔH , h_d the downstream flow depth, L_a the length of apron in the streamwise direction, L_{max} is the maximum scour length, X_{max} is the streamwise distance from the end of the apron to the maximum scour depth Z_{max} , and Z_{max_ref} is the maximum scour depth without an apron, referred to herein as the reference maximum scour depth.

Table 1. PK weir geometric characteristics.

Parameter	Value
B	1.04 m
B_b	0.52 m
$B_i = B_o$	0.26 m
N	4
P	0.42 m
P_d	1.09 m
$S_i = S_o$	0.55
T_s	0.025 m
W_i	0.248 m
W_o	0.194 m
W_i/W_o	1.280 m
W_u	0.49 m

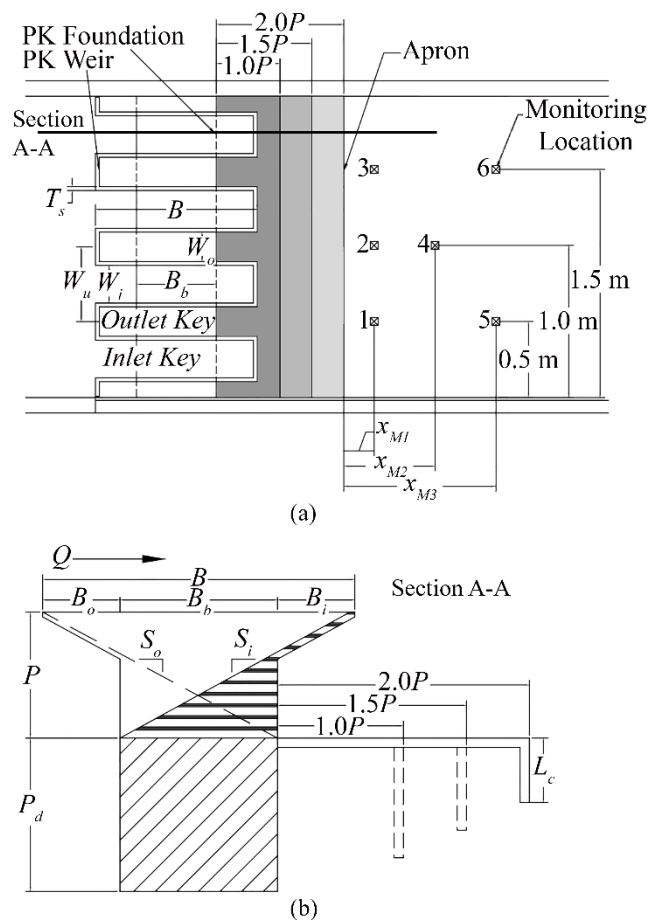


Figure 1. (a) Plan and (b) side views of weir dimensions and flume setup.

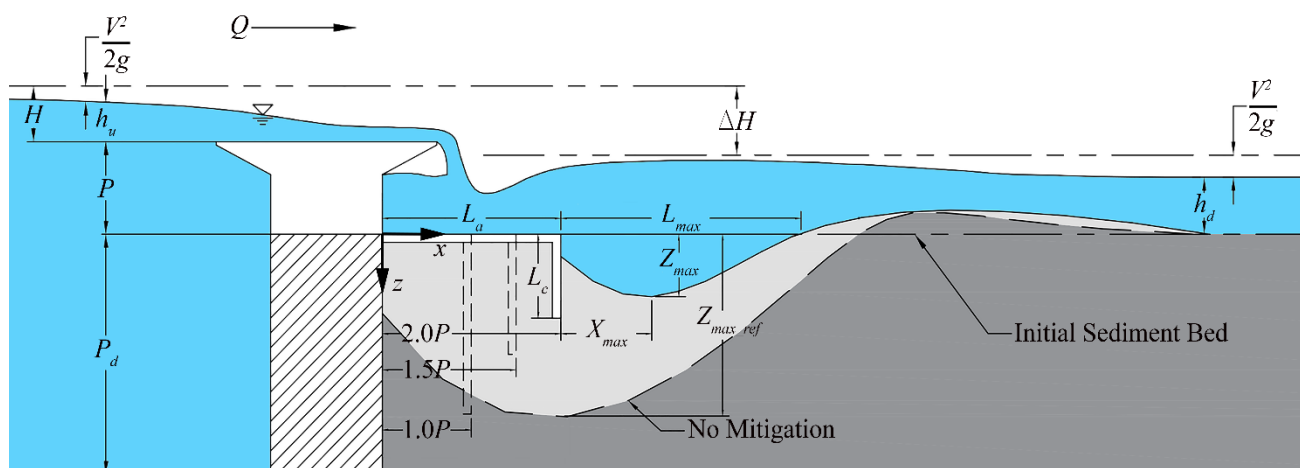


Figure 2. Profile of experimental setup with key parameters used in this study.

A calibrated venturi meter ($\pm 0.25\%$) was used to measure flow discharge (Q). A point gauge (± 0.75 mm) with a stilling well (i.e., point gauge with piezometer) was hydraulically connected two meters upstream of the weir ($4.77P$) to estimate the upstream piezometric head h_u . Conversely, the downstream water level (and, consequently, the tailwater depth h_d) was measured by using a Microsonic mic+130 ultra-sonic sensor ($\pm 1\%$) (Microsonic, Dortmund, Germany) [37,38] at 3.35 m downstream ($x/P = 8$). Initial investigations profiled the downstream water surface to select an appropriate location for computing h_d .

Scour evolution and at equilibrium was monitored by using two techniques. Namely, low-buoyancy spheres ($G = 0.53$) (see [30] for more details) were spaced vertically in the substrate at 0.1 m in vertical columns (measurement accuracy is ± 12 mm). Sphere column location was color coded, and the specific weight of the spheres was adjusted so that they would stay buried until approximately half of the sphere was exposed. Once the sphere was uncovered to this point, it quickly rose to the water surface. A GoPro Hero 7 Black high-resolution (4k) camera (GoPro, San Mateo, CA, USA) located above the channel allowed recording this process and estimate the time (t) at which each sphere was released from the bed material, i.e., the time when scour reached the depth at which the sphere was positioned. Overall, six monitoring locations were selected for the spheres and are indicated with numerical identifiers in Figure 1.

To determine equilibrium morphology, the substrate was scanned with an Intel®RealSense™ D435 depth camera (accuracy of ± 1 mm) (Intel, Santa Clara, CA, USA) [30,39,40] processed with a Utah State University (USU) custom MATLAB (vR2020) script. The camera data was cross-checked with point measurements taken on a grid layout with a point gage assembly (accuracy of ± 1 mm). This camera is capable of capturing the surface of solids or roughened or opaque water surfaces in three dimensions; its specifications are summarized in Table 2. Post-processing included 2D and 3D scour morphology plots and allowed quantifying maximum scour location (X_{max}) and its depth (Z_{max}), maximum length of the scour hole (L_{max}), and other scour features.

Table 2. Intel RealSense D435 specifications.

Feature	Detail
Global Shutter	$3 \mu\text{m} \times 3 \mu\text{m}$ pixel size
IR Stereo: FOV	$86^\circ \times 57^\circ (\pm 3^\circ)$
IR Stereo: Resolution	1280×720
RGB: FOV	$64^\circ \times 41^\circ \times 77^\circ (\pm 3^\circ)$
RGB: Resolution	1920×1080

Four apron lengths (L_a) were tested, i.e., $L_a = 0P$ (reference configuration), $1P$, $1.5P$, and $2P$, under three different combinations of Q and h_d (Table 3). Note that all tests (see

Table 5) were conducted with the lowest permissible tailwater depth in order to investigate the most critical hydraulic conditions. Each test began by slowly filling the headbox and substrate box until the weir was in a submerged condition. The target Q was set, the h_d was lowered to the lowest permissible depth, and then the timer and video recording array were initiated. Note that for certain values of Q the horizontal bed prevented the target h_d ($\sim 0.33P$) from being achieved. Multiple experiments were conducted for more than 18 h each to confirm equilibrium conditions and necessary durations for the remainder of the test matrix. More specifically, to assess the time needed to reach the equilibrium configuration, this study conducted some selected longer tests. In particular, for Substrate 2 and $Q = 600$ L/s, the reference test 15 was conducted (lasting up 1170 min, i.e., 19.5 h, see Table 5). It was observed that the differences between the equilibrium morphologies at $t = 6$ h (i.e., the same time duration of Test 18, conducted under similar hydraulic conditions) and at 19.5 h were negligible. Thus, the duration of test 18 was long enough to reach the equilibrium configuration of the bed morphology. Similar considerations apply for all the tested discharges (e.g., for $Q = 300$ L/s test 14 was conducted with duration $t = 1050$ min).

Table 3. PK Weir Scour Protection Test Matrix.

Substrate Type	Discharge Q	Headwater Ratio	Tailwater + h_d	Apron Length L_a
Substrate 1 $d_{50} = 13$ mm $d_{90} = 20$ mm $\sigma = 1.54$	150 L/s	$H/P = 0.11$	16 cm = $0.38P$	2.0P = 0.84 m
				1.5P = 0.63 m
Substrate 2 $d_{50} = 6.5$ mm $d_{90} = 9.1$ mm $\sigma = 1.30$	300 L/s	$H/P = 0.18$	17 cm = $0.41P$	1.0P = 0.42 m
				0.0P = 0.00 m *
	600 L/s	$H/P = 0.35$	22 cm = $0.52P$	2.0P = 0.84 m
				1.5P = 0.63 m
				1.0P = 0.42 m
				0.0P = 0.00 m *

† reference test tailwater, see Table 4 for all tests; * reference test without apron, or apron length $L_a = 0$.

Table 4. Experimental Results.

Run (#)	h_d (m)	Z_{max} (m)	X_{max} (m)	L_{max} (m)	V (m ³)
1 *	0.16	0.18	0.25	0.61	0.12
2 *	0.17	0.33	0.42	1.07	0.36
3 *	0.22	0.71	0.73	2.20	1.49
4	0.09	0.07	0.00	0.47	0.03
5	0.16	0.15	0.00	0.75	0.12
6	0.21	0.39	0.00	1.54	0.50
7	0.10	0.03	0.00	0.31	0.00
8	0.17	0.06	0.00	0.44	0.03
9	0.22	0.28	0.00	1.54	0.37
9R	0.23	0.23	0.00	1.45	0.37
10	0.09	No Scour	No Scour	No Scour	No Scour
11	0.15	0.06	0.00	0.36	0.02
12	0.22	0.19	0.00	1.18	0.27
13 *	0.10	0.28	0.40	1.07	0.39
14 *	0.14	0.56	0.52	1.81	1.03
15 *	0.22	1.01	1.16	3.19	3.36

Table 4. Cont.

Run (#)	h_d (m)	Z_{max} (m)	X_{max} (m)	L_{max} (m)	V (m ³)
16	0.11	0.11	0.00	0.61	0.07
17	0.16	0.20	0.00	1.15	0.26
18	0.24	0.45	0.00	1.83	0.74
19	0.11	0.06	0.00	0.47	0.03
20	0.15	0.12	0.00	1.28	0.15
21	0.25	0.34	0.00	2.37	0.56
22	0.10	0.04	0.00	0.45	0.02
23	0.15	0.11	0.00	1.02	0.12
24	0.24	0.25	0.00	3.05	0.45

R = repeat test; * reference test with no apron, or apron length $L_a = 0$.

Table 5. Testing values for each experimental run.

Run (#)	Substrate (-)	t (min)	L_a/P (-)	Q (L/s)
1 *	1	180	0.0	150
2 *	1	240	0.0	300
3 *	1	900	0.0	600
4	1	360	1.0	150
5	1	360	1.0	300
6	1	870	1.0	600
7	1	360	1.5	150
8	1	360	1.5	300
9	1	360	1.5	600
9R	1	360	1.5	600
10	1	no scour	2.0	150
11	1	120	2.0	300
12	1	360	2.0	600
13 *	2	450	0.0	150
14 *	2	1050	0.0	300
15 *	2	1170	0.0	600
16	2	840	1.0	150
17	2	780	1.0	300
18	2	720	1.0	600
19	2	240	1.5	150
20	2	840	1.5	300
21	2	990	1.5	600
22	2	480	2.0	150
23	2	600	2.0	300
24	2	720	2.0	600

R = repeat test; * reference test with no apron, or apron length $L_a = 0$.

Finally, it is worth mentioning that all the tests pertaining to $Q \leq 300$ L/s were conducted under clear water conditions [41]. More specifically, the flow intensity U/U_c was less than 1, where U and U_c are the average flow velocity and the average threshold velocity, respectively, with U_c calculated using the methodology developed by [42]. As for tests conducted with $Q = 600$ L/s and Substrate 1, tests were characterized by $U/U_c \approx 1$; Conversely, for tests with $Q = 600$ L/s and Substrate 2 (i.e., tests 15, 18, 21, and 24), U/U_c was slightly bigger than 1. Nevertheless, it was decided to also include these tests in these analyses, as their behavior in terms of the effect of apron geometry on scour characteristics was found to be essentially consistent with those of other tests. Therefore, they can provide useful information for practical applications.

3. Results

3.1. PK Weir Hydraulics

The PK weir geometry creates a 3D flow field that can be characterized by near-vertical and oblique plunging jets exiting the inlet and outlet keys, respectively. The oblique jet had a larger unit discharge than the near-vertical jet, resulting in greater shear stress acting on the granular bed in correspondence with outlet keys. In the absence of any protection measures, both jets impinge on the gravel bed [10,30]. Because of the excess of shear stress, scour evolution is initially very rapid (developing phase); successively, the kinetics of the scour evolution reduces and scour depth asymptotically reaches its maximum value. More specifically, [4] showed that, for jet-driven scour processes, the rate of material removal scales with the excess of shear stress $(\tau/\tau_c - 1)^m$, with τ indicating the shear stress, τ_c the critical shear stress, and m is a coefficient that is equal to 1.5 for non-cohesive materials according [43]. Therefore, the equilibrium configuration is achieved when $\tau = \tau_c$ and, consequently, $Z = Z_{max}$, with h_d being constant. The presence of a horizontal apron significantly modifies flow features in the downstream stilling basin. In particular, impinging jets are deflected horizontally and a more uniform distribution of the flow occurs downstream of the apron. In addition, a dissipative process may occur on the apron due to the formation of a submerged hydraulic jump. As a consequence, scour takes place downstream of the apron and is characterized by a significant reduction of the main lengths (Figure 3) in comparison with the reference case. However, depending on the tested conditions, the presence of scour may endanger the stability of the apron. Therefore, a cutoff wall is suggested to avoid undermining of the apron and a potential failure mode.



Figure 3. Photographs from experiments under identical hydraulic conditions: (a) Reference test (Run 14); (b) Scour protection via horizontal apron and cutoff wall (Run 23).

3.2. Analysis of Scour Processes

The analysis of the scour process was conducted by comparing the longitudinal scour profiles for tests with apron with that pertaining to the corresponding reference test (no apron). For the reference tests (e.g., Figure 3) some armoring occurred at equilibrium, but this was dependent upon σ and the angle of repose of the downstream slope of the scour hole, as not all smaller material was removed to result with armoring of only the largest grain sizes (e.g., d_{90}). The overall observed trend was that scour depth and maximum scour dimensions significantly decrease with L_a under identical hydraulic conditions (Figure 4 and Table 5) (note that for Run 10 no scour occurred in the stilling basin). Results evidenced that the effect of an apron is always prominent, regardless the bed material characteristics (i.e., for both Substrates 1 and 2). As mentioned in the previous section, this behavior can be explained when considering that the flow dynamics are radically different for protected basins. Both flow features and sediment transport mode exhibit similarities with that

occurring downstream of an apron caused by submerged horizontal jets. Namely, scour starts in correspondence with the edge of the structure because of the excess of shear stress. During the developing phase, bed material is mobilized and kept in suspension. Successively, when the scour hole enlarges (developed phase), the jet exiting from the apron is deflected downward. Consequently, the sediment transport mode changes, involving both suspended and bed loads. Furthermore, this study corroborates the findings of [35], which showed that the maximum scour depth is a monotonic decreasing function of the non-dimensional apron length and average diameter of the bed material. To this end are presented Figure 4a,c,e (Substrate 1) and Figure 4b,d,f (Substrate 2) where longitudinal scour profiles pertaining to tests are shown. Please note that the apron length and cutoff wall for each configuration are color matched to the corresponding maximum scour profiles. For example, in Figure 4, A $L_a/P = 1.5$ is in red, but is overlapped by $L_a/P = 1.0$ that is blue. The red scour profile (dots with dashed line) corresponds to $L_a/P = 1.5$.

The percent reduction of the maximum scour depth was quantified as $Z^*_{max} = 100(Z_{max_ref} - Z_{max})/Z_{max_ref}$, which is caused by the different apron configurations with Z_{max_ref} indicating the maximum scour depth of the corresponding reference test (i.e., without an apron). Namely, tests were grouped according to the two substrate types and Z^*_{max} was plotted as function of the non-dimensional apron length L_a/P for different densimetric Froude numbers $F_{rd90} = q/\{h_u[(G - 1)gd_{90}]^{1/2}\}$ (Figure 5a,b). Note that $q = Q/W$ and is the average unit discharge. A slight difference, depending on the inflow characteristics, can be pointed out between tests involving Substrate 1 and 2. Namely, for both the substrates Z^*_{max} is a monotonic increasing function of L_a/P . However, for tests conducted with Substrate 1 and $F_{rd90} = 3.05$ and 3.25 , Z^*_{max} becomes almost constant for $1.5 \leq L_a/P \leq 2$, i.e., it only depends upon F_{rd90} and the effect of L_a/P becomes negligible (Figure 5a). In addition, the presence of the apron prevents the scour formation for $L_a/P = 2$ and $F_{rd90} = 2.44$ (i.e., $Z^*_{max} = 100\%$, as shown in Figure 5a). A similar behavior can be pointed out for tests with Substrate 2. Overall, Z^*_{max} increases with L_a/P , whereas it slightly decreases with F_{rd90} (Figure 5b). These results corroborate the findings of [35,44,45], who found that scour processes occurring in protected stilling basins are essentially influenced by the geometry of the protection structures and the inflow conditions. The mentioned analysis allowed the derivation of the following predicting equation, valid for $0 \leq L_a/P \leq 2$:

$$Z^*_{max} = (-2.8F_{rd90} - 6.3) \left(\frac{L_a}{P}\right)^2 + (2.8F_{rd90} + 64.9) \left(\frac{L_a}{P}\right) \quad (1)$$

Figure 5c–f shows that Equation (1) provides an accurate estimation of the variable Z^*_{max} and represents a simple tool that practitioners can use to estimate scour characteristics in protected basins.

Furthermore, in this study the effect of the variable L_a was quantified regarding its effect on the maximum scour depth Z_{max} and length X_{max} , along with volume of sediment V removed under different inflow conditions and for both the substrates. In particular, Figure 6 shows that, by adding a $1.0P = L_a$ horizontal apron, the average reduction of the scour depth is approximately equal to 57%. This percentage increases with L_a and ranges between 75% and 83% for $L_a = 1.5P$ and $2.0P$, respectively (see also Table 4). It is worth remarking that the change in scour depth for $L_a = 1.5P$ and $L_a = 2.0P$ was on average 8%. It implies that, for practical applications and $F_{rd90} > 3$, an additional protection (i.e., longer apron) may only minimize scour depth marginally. Likewise, the variable L_{max} is also affected by L_a (Figure 7). However, in this case a different behavior can be pointed out depending on the sediment bed gradation and, in particular, on d_{50} . Namely, for Substrate 1, a general reduction of the scour hole length occurs by increasing L_a , regardless of the inflow conditions. Conversely, for finer bed material, the maximum scour depth seems to be less affected by the apron length, especially for higher discharges. This behavior is similar to that observed by [45] downstream of block ramps, especially for low slopes of the ramp, for which the horizontal component of the total hydrodynamic force at the ramp toe is much larger than the vertical counterpart. Namely, in the presence of a horizontal, smooth

apron, depending on the inflow conditions (i.e., especially for higher values of F_{rd90}), a hydraulic jump may not occur. Thus, the scour downstream of the apron is essentially due to a horizontal, not submerged, jet. The shear stress due to jet generally exceeds the critical counterpart, resulting in a scour formation downstream of the apron. Nevertheless, for finer bed materials, the superficial layer can be more easily transported downstream, thus modifying the overall shape of the scour hole, which becomes more longitudinally extended (Figures 4b,d,f and 7).

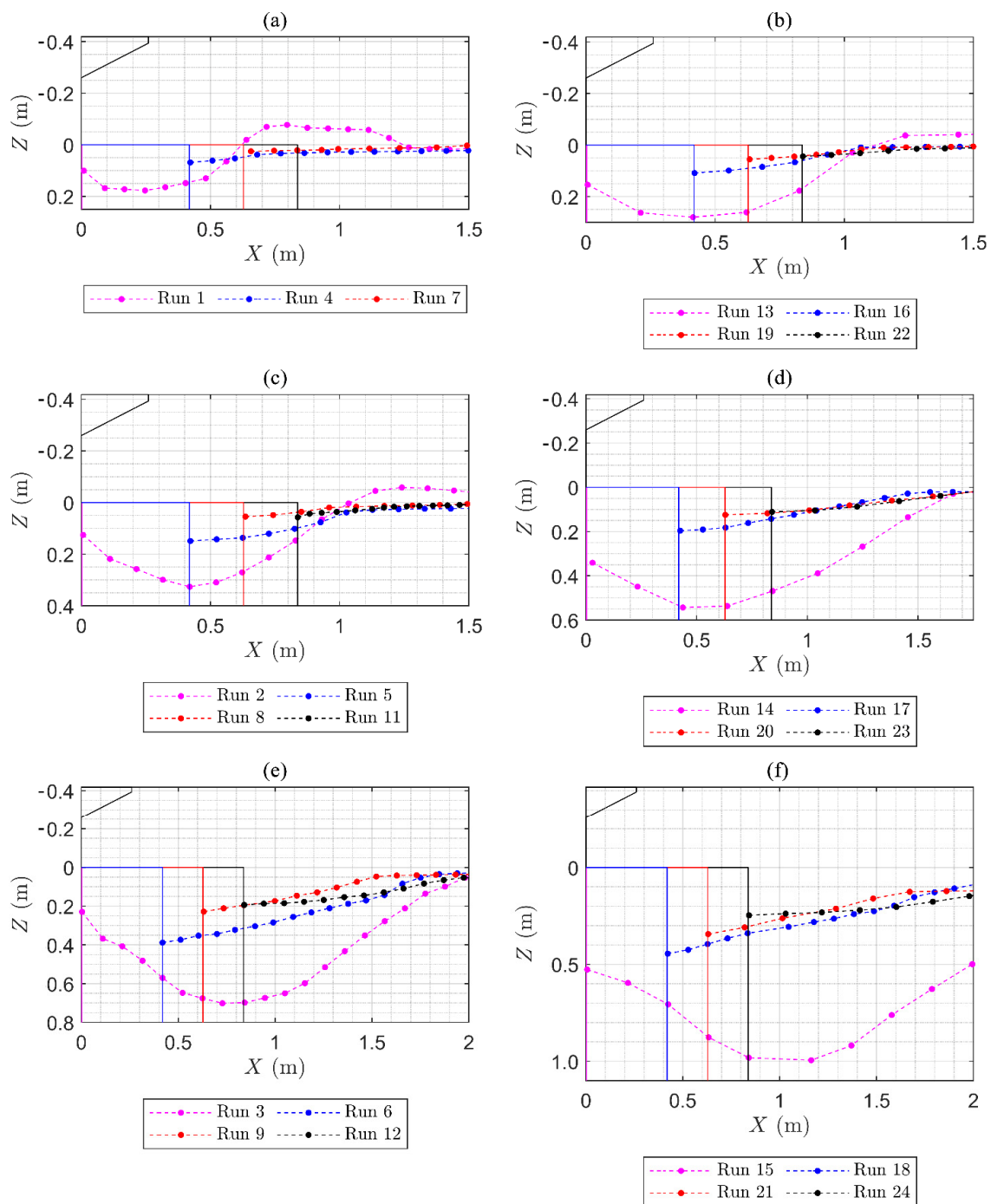


Figure 4. Comparison of longitudinal bed profiles for runs: (a) 1, 4, and 7; (b) 13, 16, 19 and 22; (c) 2, 5, 8 and 11; (d) 14, 17, 20 and 23; (e) 3, 6, 9, 9R and 12; and (f) 15, 18, 21 and 24.

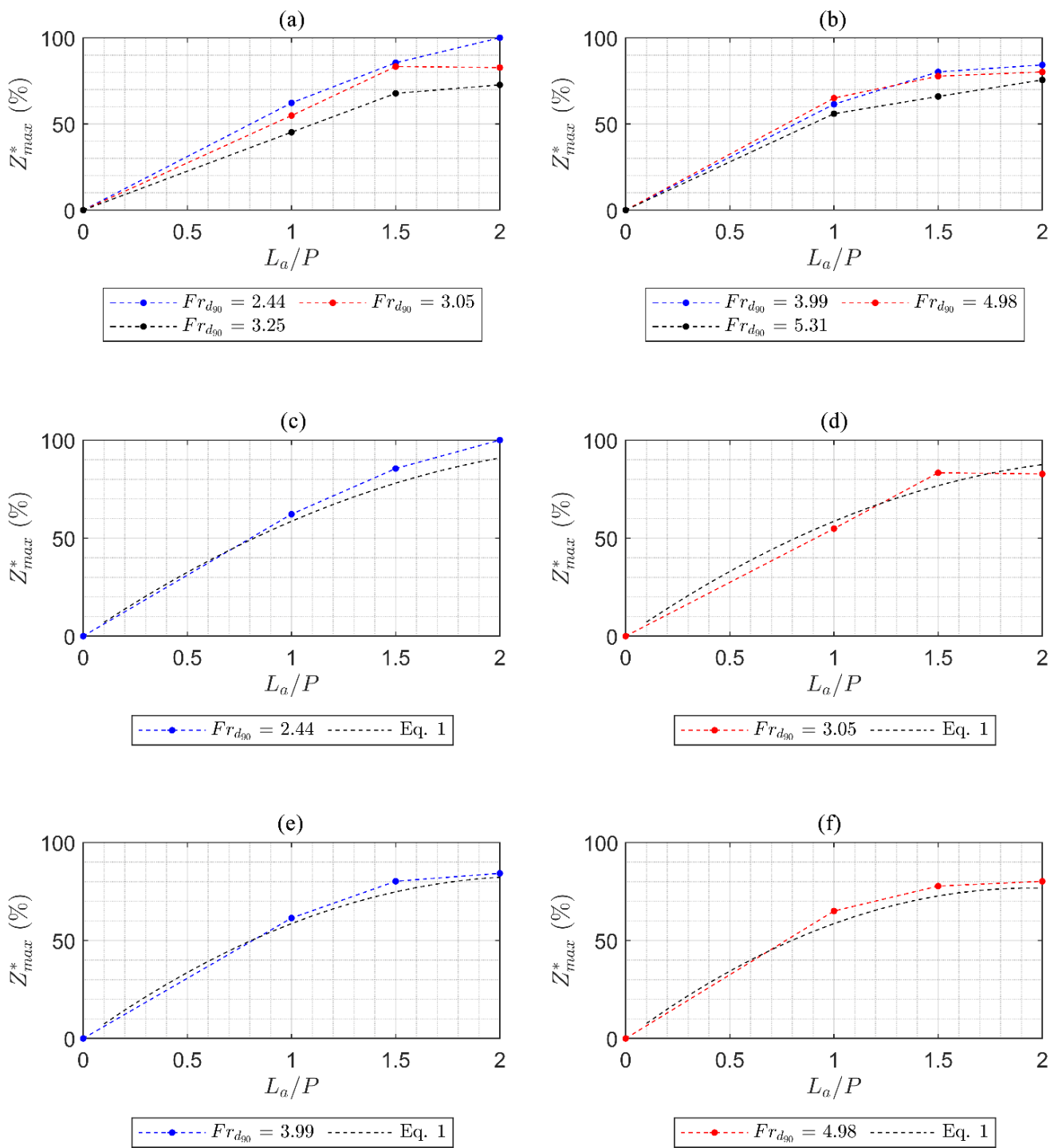


Figure 5. Z_{max}^* as function of Fr_{d90} for Substrate (a) 1 and (b) 2. Z_{max}^* as function of Fr_{d90} along with the plot of Equation (1) for Fr_{d90} = (c) 2.44, (d) 3.05, (e) 3.99, and (f) 4.98.

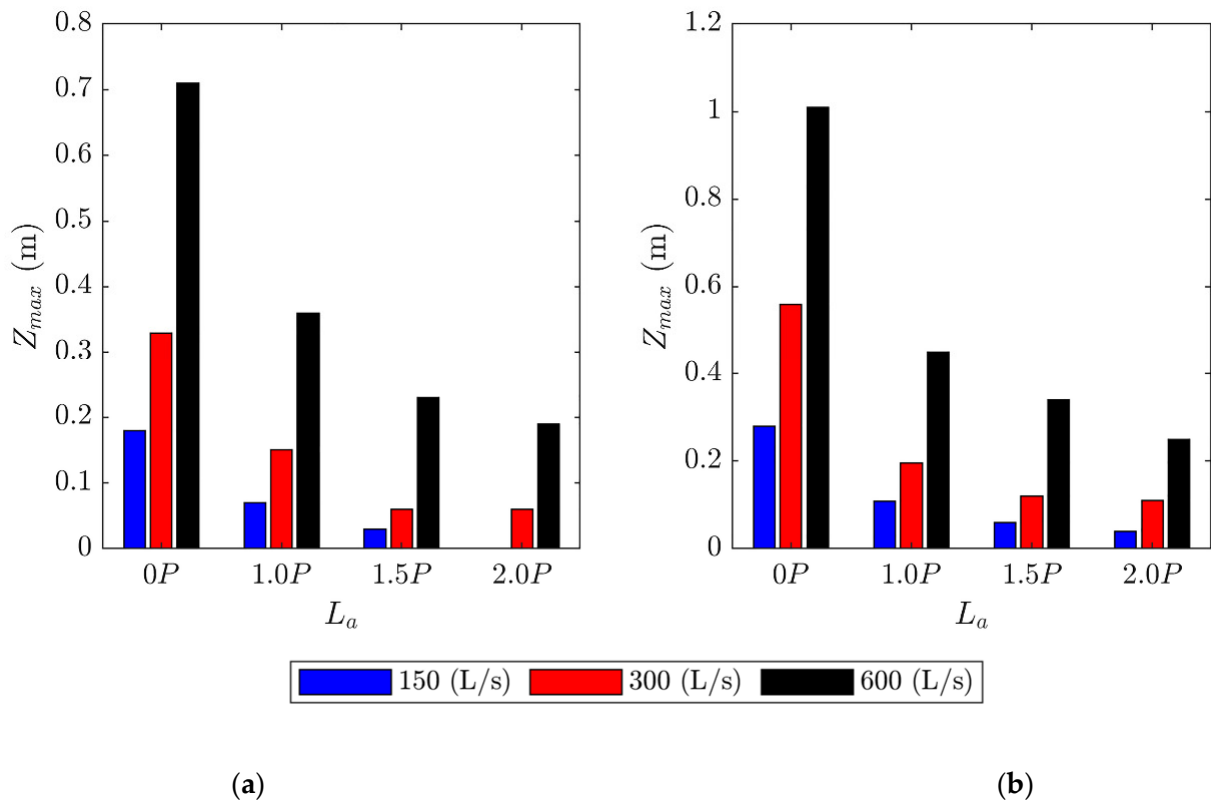


Figure 6. Effect of L_a on Z_{max} under different inflow conditions and Substrates (a) 1 and (b) 2. Note that $0P$ indicates corresponding reference tests.

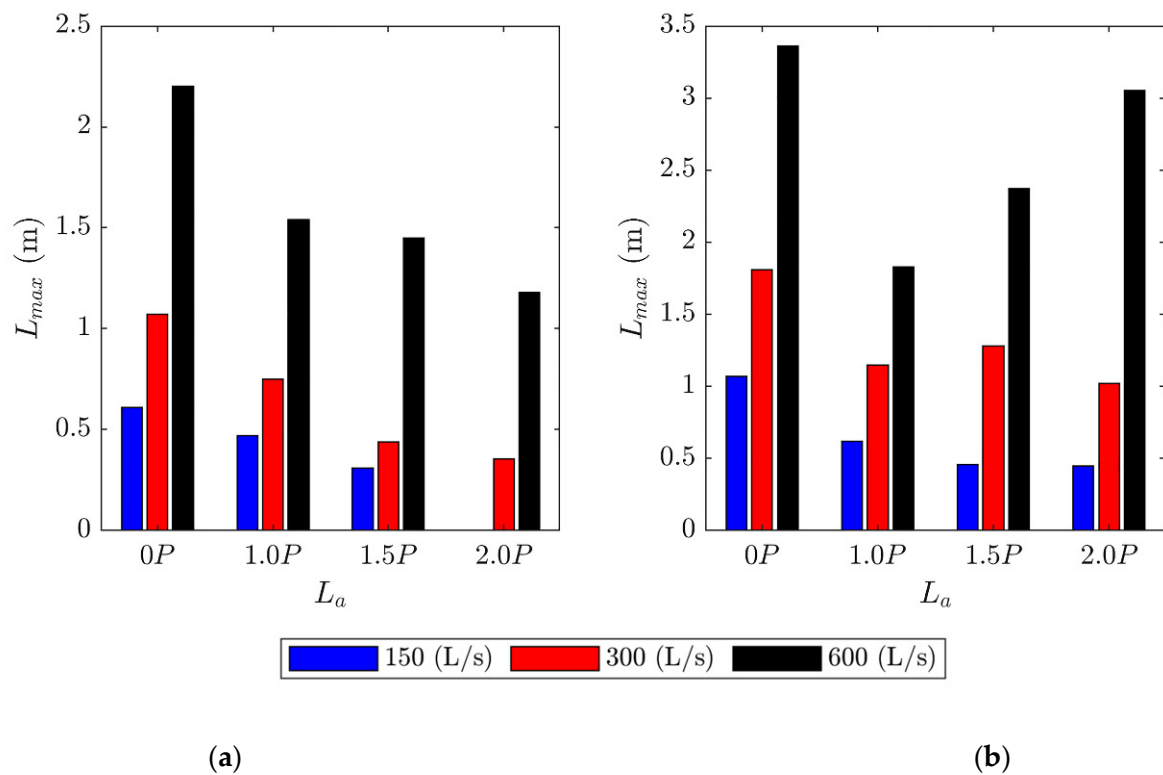


Figure 7. Effect of L_a on L_{max} under different inflow conditions and Substrates (a) 1 and (b) 2. Note that $0P$ indicates corresponding reference tests.

Finally, it does not escape attention that Equation (1) also represents a tool to estimate the maximum scour depth for protected basins. Namely, considering the definition of Z_{max}^* , Equation (1) can be re-written as follows:

$$\frac{100(Z_{max_ref} - Z_{max})}{Z_{max_ref}} = (-2.8F_{rd90} - 6.3) \left(\frac{L_a}{P}\right)^2 + (2.8F_{rd90} + 64.9) \left(\frac{L_a}{P}\right) \quad (2)$$

Or, equivalently:

$$Z_{max} = Z_{max_ref} \left\{ 1 - 0.01 \left[(-2.8F_{rd90} - 6.3) \left(\frac{L_a}{P}\right)^2 + (2.8F_{rd90} + 64.9) \left(\frac{L_a}{P}\right) \right] \right\} \quad (3)$$

valid for $2.4 \leq F_{rd90} \leq 5.3$, $0 \leq L_a/P \leq 2$, $0.11 \leq H/P \leq 0.36$, and $0.24 \leq h_d/P \leq 0.59$, but the results of this study trend to $h_d/P \leq 1.03$ (exceeds tested tailwater depth ratios presented herein). Note that the maximum scour depth in the corresponding reference test (Z_{max_ref}) can be estimated using the following Equation (4) proposed by [27]:

$$Z_{max_ref} = 0.42d_{50} \left(\frac{h_c}{d_{50}}\right)^{1.7} \left(\frac{\Delta H}{h_d}\right)^{0.3} \quad (4)$$

where $h_c = (q^2/g)^{1/3}$ is the critical depth, with q indicating the unit discharge, g the acceleration due to gravity, ΔH the change in energy head, and h_d is the tailwater depth. Figure 8 show the comparison between measured and calculated (using Equation (3)) values of the variable Z_{max} .

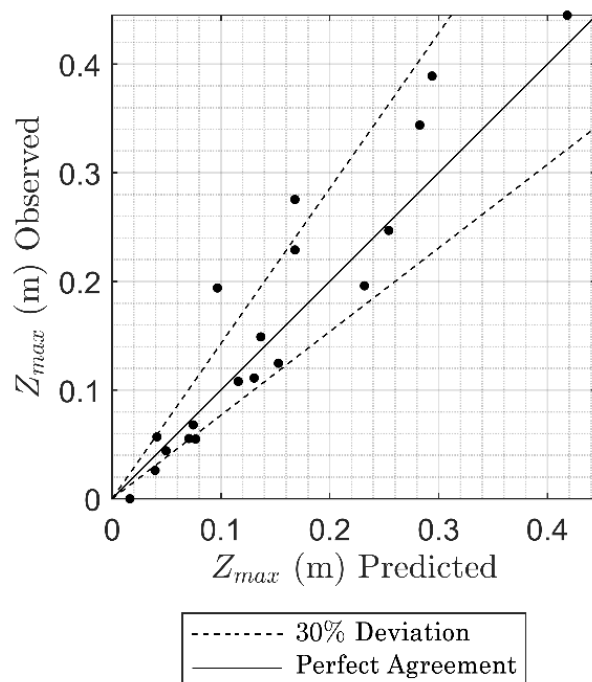


Figure 8. Comparison between measured and calculated (using Equation (3)) values of the maximum scour depth Z_{max} for protected basins, with 30% bounding lines referencing Z_{max} Observed.

3.3. Apron and Cutoff Wall Design Guidance

The design and construction of an apron and cutoff wall must first consider a practical perspective of the entire structure design and how it may be constructed. Specifically, the PK Weir would require a foundation if placed in a river where it cannot be founded on competent rock. Thus, an economic analysis coupled with corresponding risks would inform the selection of (a) a deeper PK weir foundation while allowing a scour hole versus

(b) designing downstream protection as part of the structure. Thus, when considering scour protection, the proper design of an apron and cutoff wall can help protect run-of-river structures from detrimental scour events associated with hydraulic conditions during flood events. In the previous section, it was shown that if Z^*_{max} exceeds 75%, the effect of the apron length becomes negligible, i.e., a further longitudinal extension of the apron results in a very marginal additional reduction of the scour depth (Figure 5a,b). Therefore, for practical applications, it can be reasonably assumed that a design value of the apron length for which $Z^*_{max} = 75$. Consequently, Equation (2) can be rearranged as follows:

$$(-2.8F_{rd90} - 6.3) \left(\frac{L_a}{P} \right)^2 + (2.8F_{rd90} + 64.9) \left(\frac{L_a}{P} \right) - 75 = 0 \quad (5)$$

and, for $0 \leq L_a/P \leq 2$:

$$\frac{L_a}{P} = \frac{-(2.8F_{rd90} + 64.9) + \sqrt{(2.8F_{rd90} + 64.9)^2 + 300(-2.8F_{rd90} - 6.3)}}{2(-2.8F_{rd90} - 6.3)} \quad (6)$$

Equation (6) provides a tool to estimate the optimum relative length of the apron L_a/P in order to maximize the scour reduction and minimize the construction cost. Note that Equation (6) is valid in the same ranges of parameters of Equation (3). It is worth remarking that Equation (6) does not depend on the tailwater level, which is one of the most important parameters in scour processes as the shear stress acting on the movable bed scales with the inverse of the sum of the water depth and scour depth. However, as mentioned in one of the previous sections, the range of variation of this parameter was relatively limited. Consequently, under tested conditions, its effect was found to be negligible. Overall, Equation (6) represents a useful tool as it can provide good estimations of the scour characteristics under most critical conditions (i.e., design condition). However, further investigations are needed to assess the effect of the tailwater depth. Figure 9 shows the plot of Equation (6), i.e., L_a/P as function of the densimetric Froude number F_{rd90} .

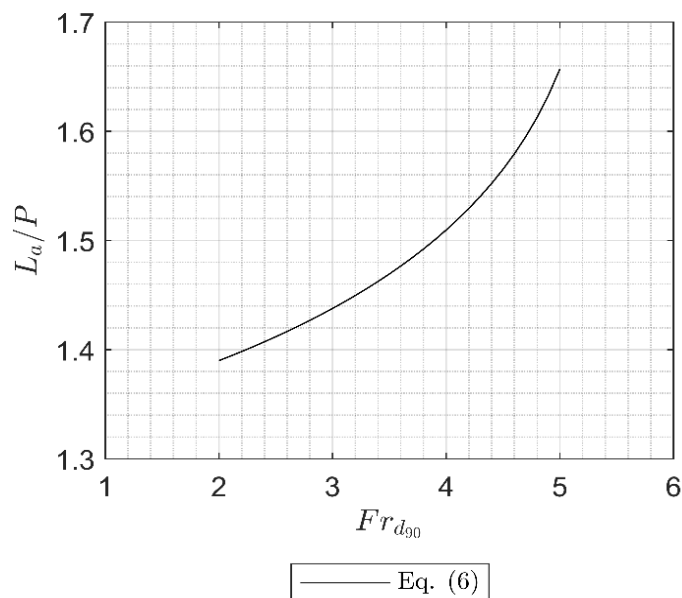


Figure 9. Optimal design values of the variable L_a/P as function of F_{rd90} .

Finally, in practice for erodible foundations a cutoff wall is often included both for the PK weir and then again at the end of a concrete apron or slab to protect against undermining. Based on the results of these tests, the maximum scour depth occurs in correspondence or in proximity of the edge of the apron. Therefore, the length or depth L_c

of a cutoff wall should be designed in such a way that it is larger than the maximum scour depth Z_{max} calculated using Equation (3). To this end, the following is proposed:

$$L_c = FS \times Z_{max} \quad (7)$$

where FS is the factor of safety selected by the designer according to site conditions and project objectives; note that when considering the deviation between measured and calculated values of Z_{max} , it is less than 30% for nearly all cases (see Figure 8) and thus a minimum FS would be 1.3. It is worth mentioning that the length of the cutoff wall L_c accounts for both inflow conditions and geometry of the structure, as such variables are embedded in Z_{max} . Further considerations for selection of L_c might include depth to a nonerodable geologic feature to key into, any relevant field observations, and balancing risks and project economy (i.e., excavation, dewatering, control of water, etc.).

Finally, it is worth remarking upon some site-specific design details that are not discussed herein, such as the means and methods of construction (i.e., in the dry with diversion or in the wet with excavation, sheet piles, etc.), the selection of the apron elevation (herein set at the base of the PK weir), the structural design of the apron and cutoff wall (dynamic forces, uplift pressures and loading moments, structural joints and connections, abrasion, etc.), and any changes to the existing mobile bed elevation downstream of the structure such as by general bed degradation independent of the weir, lateral channel migration, or downstream-instigated headcuts that may migrate upstream to the PK weir apron, etc. In addition, all the proposed equations from this study should be validated using field data, as they can be subjected to scale effects, regardless of the model scale. However, for the present study, a large laboratory flume was used. Considering that the width of natural streams/rivers (where such structures are located) is generally less than 50 m, the model scale can be assumed to be bigger than 1:25. Furthermore, tests were conducted for a Reynolds number greater than 50,000. Under such conditions, [46] showed that scale effects are negligible.

4. Conclusions

Limited published guidance is available for designing a minimal apron and cutoff wall lengths to protect or mitigate local scour at the toe of a PK weir. This encouraged a large-scale physical model study on the effects of scour at PK weirs with and without aprons and cutoff walls. From this study the following conclusions have been made:

- Scour depths in the two tested noncohesive gravel materials without an apron and cutoff wall were significant.
- Jets ensuing from the PK weir structure diffused over the apron and cause horizontal jet scour downstream of the apron.
- Adding a $1.0P$ long apron can reduce scour by an average of 61%, adding a $1.5P$ long apron can reduce scour by an average of 75%, and adding a $2.0P$ apron can reduce scour by an average of 83%. Thus, apron length L_a can be optimized considering PK weir hydraulics and geometry with geologic conditions at PK weir toe.
- Equations (3) and (6) were created to estimate L_a , Z_{max} downstream of an apron along with Equation (4), and Equation (7) was created to estimate L_c to protect the structure from scour undermining. Note that Equations (3) and (6) are considered valid for $2.4 \leq F_{rd90} \leq 5.3$, $0 \leq L_a/P \leq 2$, $0.11 \leq H/P \leq 0.36$, and $0.24 \leq h_d/P \leq 1.03$. All proposed equations should be validated using field data.
- For this study, it was determined that there was an 8% difference in the reduction of scour from a $1.5P$ apron length to a $2.0P$ apron length, and a $1.5P$ apron may be an adequate and cost-effective length to minimize scour. Note that as the substrate diameter decreases the potential for scour depth and length downstream of the apron will increase.
- Although the facility tested at USU was quite large and might be considered a 1:5 to 1:10 scaled model, quantification of any scale effects requires additional investigation.

As with other laboratory-scale scour studies, there are multiple limitations to this study, yet there are ways that practitioners can overcome these limitations. First, the steady-state nature of the testing: To overcome this limitation, practitioners can use Z_{max} values as conservative design values. Another limitation was that only three Q and one h_d conditions were tested in this study. To overcome this limitation, practitioners could use graphical means to interpolate potential Z_{max} values based on the rating curves provided and might adjust their FS if tailwater depths are greater. Further, results may be scaled using the densimetric Froude number. Furthermore, only two relatively uniform substrate materials were studied. Practitioners could use methods similar to the Erodibility Index method of [47] to scale geologic material strengths in the field to a noncohesive laboratory-scale material, such as was selected and tested herein. Additionally, these results and equations only directly apply to horizontal aprons without a sill and very mild river slopes or energy gradients. Lastly, only one PK weir geometry was tested with q estimated as Q/W .

Author Contributions: Conceptualization, B.M.C., W.L., and M.P.; methodology, B.M.C., W.L., and M.P.; software, W.L.; validation, B.M.C., W.L., and M.P.; formal analysis, B.M.C., W.L., and M.P.; investigation, B.M.C., W.L., and M.P.; resources, B.M.C.; data curation, W.L.; writing—original draft preparation, B.M.C., W.L., and M.P.; writing—review and editing, B.M.C. and M.P.; visualization, W.L.; supervision, B.M.C.; project administration, B.M.C.; funding acquisition, B.M.C. All authors have read and agreed to the published version of the manuscript.

Funding: For this research, the second author (Brian Crookston) was funded by USGS Grant 104b through the Utah Water Research Laboratory and by a generous private donation by D. Campbell.

Institutional Review Board Statement: Not applicable.

Informed Consent Statement: Not applicable.

Data Availability Statement: Some or all data, models or code that support the findings of this study are available at <https://digitalcommons.usu.edu/etd/8090/> (accessed on 4 March 2021) or from the corresponding author upon reasonable request.

Acknowledgments: The second author (Brian Crookston) thanks D. Campbell for his generous private donation to support this study.

Conflicts of Interest: The authors declare no conflict of interest. The funders had no role in the design of the study; in the collection, analyses, or interpretation of data; in the writing of the manuscript, or in the decision to publish the results.

References

1. Laursen, E.M. Observations on the Nature of Scour. In *Proceedings 5th Hydraulics Conference Bulletin*; University of Iowa: Iowa City, IA, USA, 1952; pp. 179–197.
2. Ettema, R.; Yoon, B.; Nakato, T.; Muste, M. A review of scour conditions and scour-estimation difficulties for bridge abutments. *Water Eng.* **2004**, *8*, 643–650. [CrossRef]
3. Zehe, E.; Becker, R.; Bárdossy, A.; Plate, E. Uncertainty of simulated catchment runoff response in the presence of threshold processes: Role of initial soil moisture and precipitation. *J. Hydrol.* **2005**, *315*, 183–202. [CrossRef]
4. Bombardelli, F.A.; Palermo, M.; Pagliara, S. Temporal evolution of jet induced scour depth in cohesionless granular beds and the phenomenological theory of turbulence. *Phys. Fluids* **2018**, *30*, 085109. [CrossRef]
5. Palermo, M.; Pagliara, S.; Bombardelli, F.A. Theoretical Approach for Shear-Stress Estimation at 2D Equilibrium Scour Holes in Granular Material due to Subvertical Plunging Jets. *J. Hydraul. Eng.* **2020**, *146*, 04020009. [CrossRef]
6. Hoffmans, G.J.C.M.; Verheij, H.J. *Scour Manual*; Balkema, A.A., Ed.; Taylor and Francis Group: Rotterdam, The Netherlands, 1997.
7. Adduce, C.; Sciortino, G. Scour due to a horizontal turbulent jet: Numerical and experimental investigation. *J. Hydraul. Res.* **2006**, *44*, 663–673. [CrossRef]
8. Dey, S.; Raikar, R. Scour below a High Vertical Drop. *J. Hydraul. Eng.* **2007**, *133*, 564–568. [CrossRef]
9. Ben Meftah, M.; Mossa, M. New Approach to Predicting Local Scour Downstream of Grade-Control Structure. *J. Hydraul. Eng.* **2020**, *146*, 04019058. [CrossRef]
10. Lantz, W.; Crookston, B.M.; Palermo, M. Flood Infrastructure: Localized Scour at Piano Key Weirs. In *Dam Safety 2020: Conference Proceedings*; Association of State Dam Safety Officials: Lexington, KY, USA, 2020.
11. United States Department of the Interior Bureau of Reclamation (USBR). *Engineering Monograph No. 25: Hydraulic Design of Stilling Basins and Energy Dissipators*; U.S Bureau of Reclamation: Denver, CO, USA, 1984.

12. Thompson, P.; Kilgore, R. Hydraulic Design of Energy Dissipators for Culverts and Channels. In *Federal Highway Administration*; National Highway Institute: Washington, DC, USA, 2006.
13. United States Department of Agriculture (USDA). *The SAF Stilling Basin*; U.S. Government Printing Office: Washington, DC, USA, 1959.
14. Peterka, J. *Hydraulic Design of Stilling Basins and Energy Dissipators*; Bureau of Reclamation: Denver, CO, USA, 1958.
15. Vischer, D.L.; Hager, W.H. *Energy Dissipators: IAHR Hydraulic Structures Design Manuals 9*; Taylor and Francis: Abingdon, UK, 1995.
16. Novak, P.; Moffat, A.; Nalluri, C.; Narayanan, R. *Hydraulic Structures*, 4th ed.; E & FN Spon: Abingdon, UK, 1995.
17. Khatsuria, R.M. *Hydraulics of Spillways and Energy Dissipators*; Marcel Dekker: New York, NY, USA, 2005.
18. Hager, W.H.; Schleiss, A.J.; Boes, R.M.; Pfister, M. *Hydraulic Engineering of Dams*; CRC Press: London, UK, 2020.
19. Ho Ta Khanh, M.; Truong, C.H.; Nguyen, T.H. *Main Results of the P.K Weir Model Tests in Vietnam (2004–2010)*; Labyrinth and Piano Key Weirs: PKW 2011; Taylor and Francis Group: London, UK, 2011; pp. 191–198.
20. Crookston, B.M.; Erpicum, S.; Tullis, B.P.; Laugier, F. Hydraulics of Labyrinth and Piano Key Weirs: 100 Years of Prototype Structures, Advancements, and Future Research Needs. *J. Hydraul. Eng.* **2019**, *145*, 02519004. [[CrossRef](#)]
21. Urban and Environmental Engineering (UEE). World Register of Piano Key Weirs Prototypes. Liege Universite. 2021. Available online: https://www.uee.uliege.be/cms/c_5026433/en/world-register-of-piano-key-weirs-prototypes (accessed on 11 March 2021).
22. Schleiss, A.J. *From Labyrinth to Piano Key Weirs—A Historical Review*; Labyrinth and Piano Key Weirs: PKW 2011; Taylor and Francis Group: London, UK, 2011; pp. 3–16.
23. Ribeiro, M.L.; Pfister, M.; Schleiss, A.J.; Boillat, J.L. Hydraulic design of A-Type Piano Key Weirs. *J. Hydraul. Res.* **2012**, *50*, 400–408. [[CrossRef](#)]
24. Machiels, O.; Piroton, M.; Pierre, A.; Dewals, B.; Erpicum, S. Experimental parametric study and design of Piano Key Weirs. *J. Hydraul. Res.* **2014**, *52*, 326–335. [[CrossRef](#)]
25. López-Soto, J.; Wibowo, J.; Molina-Bas, O. Cost Reduction in Dam Infrastructure Using Arced Labyrinth Spillways. In *Construction Research Congress 2016*; San Juan, Puerto Rico, American Society of Civil Engineers (ASCE): Reston, VA, USA, 2016. [[CrossRef](#)]
26. Laugier, F.; Vermeulen, J.; Lefebvre, V. *Overview of Piano Key Weirs Experience Developed at EDF during the Past Few Years*; Labyrinth and Piano Key Weirs II: PKW 2013; Taylor and Francis Group: London, UK, 2013; pp. 213–226.
27. Jüstrich, S.; Pfister, M.; Schleiss, A.J. Mobile Riverbed Scour Downstream of a Piano Key Weir. *J. Hydraul. Eng.* **2016**, *142*, 04016043. [[CrossRef](#)]
28. Pfister, M.; Jüstrich, S.; Schleiss, A.J. *Toe-Scour Formation at Piano Key Weirs*; Labyrinth and Piano Key Weirs III—PKW 2017; Taylor and Francis Group: London, UK, 2017; pp. 147–156.
29. Palermo, M.; Crookston, B.; Pagliara, S. Analysis of Equilibrium Morphologies Downstream of a PK Weir Structure. In *World Environmental and Water Resources Congress 2020*; American Society of Civil Engineers (ASCE): Reston, VA, USA, 2020; pp. 43–51. [[CrossRef](#)]
30. Lantz, W. A Laboratory Study on the Geometric Effects of Piano Key Weirs on Scour for Non-Cohesive Substrates and Simple Mitigation Techniques. Master's Thesis, Utah State University, Logan, UT, USA, 2021. [[CrossRef](#)]
31. Yazdi, A.M.; Hoseini, S.A.; Nazari, S.; Amanian, N. Effects of weir geometry on scour development in the downstream of Piano Key Weirs. *Water Supply* **2021**, *21*, 289–298. [[CrossRef](#)]
32. Hassan, N.M.K.N.; Narayanan, R. Local Scour Downstream of an Apron. *J. Hydraul. Eng.* **1985**, *111*, 1371–1384. [[CrossRef](#)]
33. Chatterjee, S.S.; Ghosh, S.N.; Chatterjee, M. Local Scour due to Submerged Horizontal Jet. *J. Hydraul. Eng.* **1994**, *120*, 973–992. [[CrossRef](#)]
34. Sarkar, A.; Dey, S. Scour downstream of aprons caused by sluices. *Proc. Inst. Civ. Eng. Water Manag.* **2005**, *158*, 55–64. [[CrossRef](#)]
35. Dey, S.; Sarkar, A. Scour Downstream of an Apron Due to Submerged Horizontal Jets. *J. Hydraul. Eng.* **2006**, *132*, 246–257. [[CrossRef](#)]
36. Erpicum, S.; Laugier, F.; Boillat, J.L.; Piroton, M.; Reverchon, B.; Schleiss, A.J. *Labyrinth and Piano Key Weirs—PKW 2011*; CRC Press: London, UK, 2011.
37. Microsonic. “mic+ 130/IU/TC.” mic+ Ultrasonic Sensors. 2021. Available online: <https://www.microsonic.de/en/distance-sensors/cylindrical/micplus/standard-sensors/standard-sensors/micplus130iutc.htm> (accessed on 4 March 2021).
38. Zhang, G.; Valero, D.; Bung, D.; Chanson, H. On the estimation of free-surface turbulence using ultrasonic sensors. *Flow Meas. Instrum.* **2018**, *60*, 171–184. [[CrossRef](#)]
39. Intel. “Depth Camera D435.” Intel RealSense. 2021. Available online: <https://www.intelrealsense.com/depth-camera-d435/> (accessed on 4 March 2021).
40. Bung, D.B.; Crookston, B.M.; Valero, D. Turbulent free-surface monitoring with an RGB-D sensor: The hydraulic jump case. *J. Hydraul. Res.* **2020**, 1–12. [[CrossRef](#)]
41. Oliveto, G.; Hager, W.H. Temporal Evolution of Clear-Water Pier and Abutment Scour. *J. Hydraul. Eng.* **2002**, *128*, 811–820. [[CrossRef](#)]
42. Neill, C.R. Note on Initial Movement Of Coarse Uniform Bed-Material. *J. Hydraul. Res.* **1968**, *6*, 173–176. [[CrossRef](#)]
43. Julien, P.Y. *Erosion and Sedimentation*, 2nd ed.; Cambridge University Press: Cambridge, UK, 2010.

-
44. Pagliara, S.; Palermo, M. Scour control and surface sediment distribution downstream of block ramps. *J. Hydraul. Res.* **2008**, *46*, 334–343. [[CrossRef](#)]
 45. Pagliara, S.; Roy, D.; Palermo, M. 3D plunge pool scour with protection measures. *J. Hydro-Environ. Res.* **2010**, *4*, 225–233. [[CrossRef](#)]
 46. Heller, V. Scale effects in physical hydraulic engineering models. *J. Hydraul. Res.* **2011**, *49*, 293–306. [[CrossRef](#)]
 47. Annandale, G.W. Erodibility. *J. Hydraul. Res.* **1995**, *33*, 471–494. [[CrossRef](#)]